Journal of Power Sources 183 (2008) 193–204

Contents lists available at ScienceDirect

Journal of Power Sources

journal homepage: www.elsevier.com/locate/jpowsour

Measurements of current and water distribution for a micro-PEM fuel cell with different flow fields

Shou-Shing Hsieh*, Yi-Ji Huang

Department of Mechanical and Electro-Mechanical Engineering, National Sun Yat-Sen University, Kaohsiung 80424, Taiwan, ROC

ARTICLE INFO

Article history:
Received 27 February 2008
Received in revised form 22 April 2008
Accepted 22 April 2008
Available online 4 May 2008

Keywords:
Current distribution
Water formation
Flow field plate
Segmented mapping method

ABSTRACT

Time-dependent measurements for the mapping of current distribution via a segmented flow field plate approach in a micro-proton exchange membrane (PEM) fuel cell were conducted and the effects of flow field configuration were studied and discussed under fixed operating conditions. The results show that, among four flow fields studied herein, the interdigitated flow channel has the most uniform transient current distribution with a much higher water content at an early phase (say $t < 0.5$ h) than those of the other three channels: serpentine, mesh and parallel, indicating an adequate oxygen concentration of the airflow on the cathode. In addition, the effect of water content on current distribution was also examined and discussed. It was found that the volume of water in flow channels could reach a steady value of 45% for all four flow fields after a 3-h operation.

1. Introduction

Proton exchange membrane (PEM) fuel cells have long been recognized as one of the most promising candidates for future power generating systems, especially in portable electronic devices. This is because the PEM fuel cell presents a high power density and operates at a relatively low temperature, two qualities which make it ideal for portable systems. However, the performance of low-temperature fuel cells, like PEM fuel cells, needs substantial improvement concerning several technical issues.

For instance, at low current density, the activation over potential is large, and at high current density, other problems may be generated, like the transport limitation of oxygen to the catalyst sites. This results in heterogeneous current distribution over the cathode. In addition, effective water removal is necessary to achieve high cell performance, since water may accumulate on the cathode due to water production and water transport resulting from the electro-osmotic drag.

In order to determine water transport and current density variations in a fuel cell, it is quite important to measure local current distributions. Most examples of current distribution inside a fuel cell are studied via numerical simulations. Only few experimental studies have been reported [1–4]. One previously developed approach to obtain the current distribution is through the use of a segmented fuel cell [5]; the segmented cell is similar to an ordinary fuel cell with the exception that one of the electrodes is divided into small electrodes. Each small electrode can be interrogated for current, voltage, and resistance. This approach permits the mapping of the current distribution across the surface of the electrode.

In a PEM fuel cell, hydrogen and oxygen react electrochemically to water, generating electricity and heat [6]. A single PEM fuel cell consists of a membrane electrode assembly (MEA) sandwiched between gas diffusion layers (GDLs) and flow field plates into which gas channels have been machined. At the cathode–membrane–electrode interface, oxygen is reduced electrochemically, yielding water as the byproduct. The amount of water produced is directly proportional to the current. Since the cathode has to face the electrode flooding problem, it consequently results in poor cell performance. In fact, an efficient fuel cell design requires a comprehensive understanding of liquid phase water transport throughout the cathode flow channel.

In conventional PEM fuel cells, the water accumulation in the cathode flow channel for parallel/or serpentine configuration constitutes a more serious than that for the interdigitated flow channel with air operation. Such phenomena still occur in the present micro-PEM fuel cells. In fact, it has been shown [7] that different flow channel configuration designs, such as the interdigitated flow channel, help to induce forced water removal from the open structure of the gas diffusion layer [8]; however, it does induce higher pressure drops between the inlet and outlet. In addition, in order to achieve stable and homogenous performance in the entire area

* Corresponding author. Tel.: +886 7 5252000x4215; fax: +886 7 5254215.
E-mail address: sshsieh@faculty.nsysu.edu.tw (S.-S. Hsieh).

0378-7753/$ – see front matter © 2008 Elsevier B.V. All rights reserved.
doi:10.1016/j.jpowsour.2008.04.065

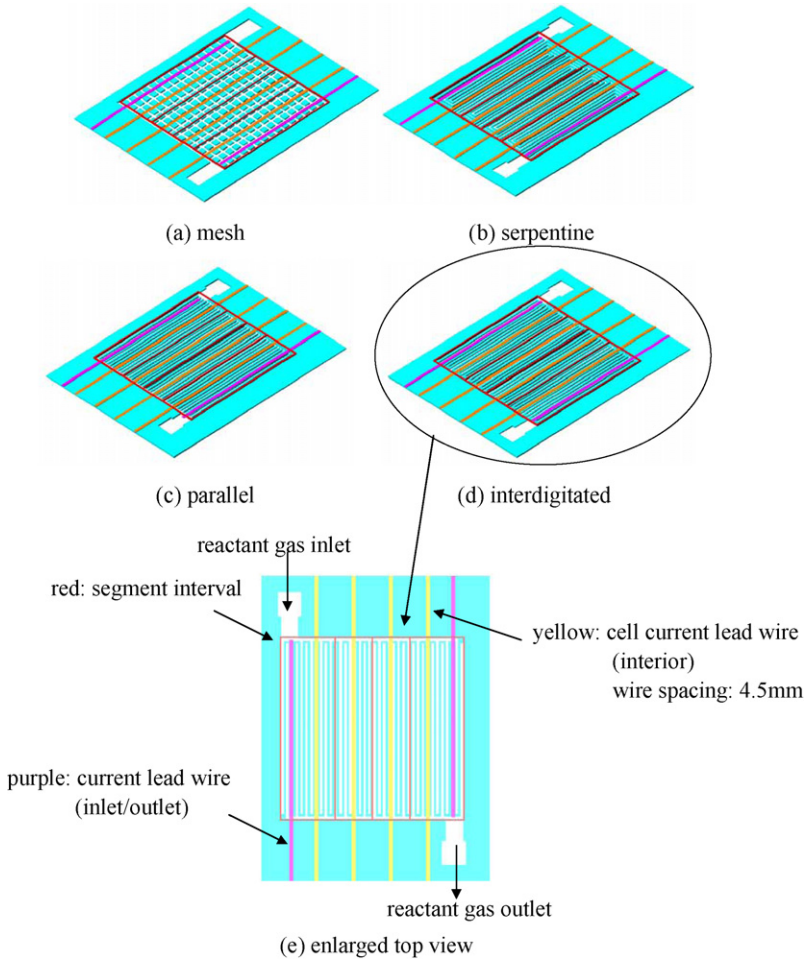

Fig. 1. Segmented anode/cathode flow fields for four different flow configuration (flow field material either silicon wafer or copper, when water formation visualization was taken).

of the flow field plate, the mass flow rate of air should be such that oxygen concentration remains as uniform as possible, while simultaneously maintaining water balance [1]. These two factors are related to the water and thermal management of a fuel cell, while current is drawn from the cell.

Although direct flow visualization requires a special cell design, it is still a very attractive experimental technique since non-intrusive access to the channels would offer high temporal and/or spatial resolution. While such a visualization technique is primarily employed in testing qualitative data, visualization has assisted in clarifying the influence of water formation and accumulation on fuel cell current distribution.

In this study, time-dependent in situ measurements of local current distribution for a 5 cm^2 H_2/air micro-PEM fuel cell with four different flow channels (mesh, parallel, serpentine, and interdigitated), were conducted via the segmented flow field plate approach, the most suitable method for PEM fuel cell [3], to obtain details inside the fuel cell on a local level for distribution of current, heat, and water. Furthermore, water accumulation measurements were made to examine water flooding on local current distribution as well as cell performance.

2. Experimental

In the study, we focus on a forced-air cathode design. Its essential characteristics include: four different flow channel configurations: parallel, serpentine, interdigitated, and mesh type that extend from one edge of the flow field plate to the other. The ends of the channels are open to the ambient air. Oxygen is transported to the electrode directly from ambient air by force driven by compressor.

2.1. Cell design and measurement setup

The segmented cell contained a one-piece cathode with an active area of 5 cm^2 and was divided into four (4) segments each with 1.25 cm^2 active surface area. The matrix of the plate was made of SU-8. Fig. 1 shows one of the segmented flow fields for four different flow field geometries. It has four (4) pass with ten (10) parallel and serpentine fashions. Also shown in Fig. 1(a)–(d) is a schematic of the segmented cell setup in consecutive order from gas inlet to gas outlet for each flow configuration, respectively. Fig. 1(e) shows an enlarged view of an interdigatated flow configuration.

The current lead wires of each segment were threaded through separate standard data logger (Agilent 34970A). The lead flat wires had a thickness of 0.01 mm with a 0.5 mm × 38 mm area and kept as short as possible to minimize the ohmic losses. Each lead wire was connected through a 1 mΩ high-resolution resistor to a load unit. The voltage drop over each resistance was monitored with a data logger, which was further controlled with a PC, as shown in Fig. 2. The area specific current density i_i could be calculated from the corresponding voltage readings v_i measured over 0.1 Ω resistors by

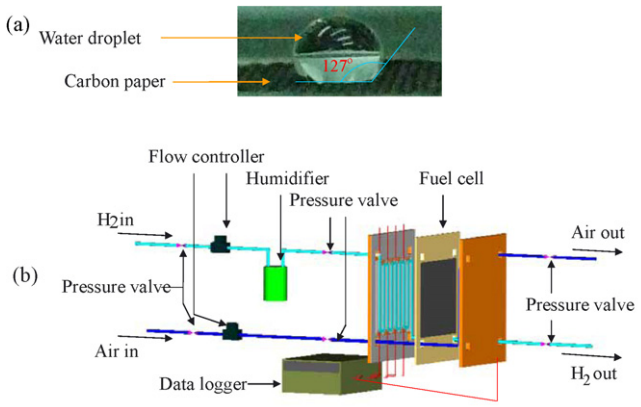

Fig. 2. Contact angle measurement and the schematic of the present measurement setup.

using the Ohm's law followed by Noponen et al. [1], as indicated in Eq. (1) below. The measurement time was approximately 0.1 s for each segment:

$$i_i = \frac{1000 v_i}{a_i R} \quad (1)$$

where a_i is the area (the active area divided by the number of measurement pin) from which a current collector copper pin collects current i_i, R is the measurement resistance, and the subscript i defines the position of a measurement pin. After substituting the proper values in Eq. (1), the equation can be further simplified as

$$i_i = 9876.5\, v_i \quad (2)$$

Here v_i has the unit of volt and i_i is mA cm^{-2}. Table 1 lists the relevant parameters involved and summarizes the experimental conditions used in this study. Details not included in the table are entered in the text.

Table 1
Experimental parameters operating conditions

Substrate plate	Silicon wafer	
Photo resist	SU-8 2100	
MEA	Nafion 117	
Catalyst	Pt/C	0.5 mg cm^{-2}
GDL	Carbon paper	0.29 mm
Flow plate	Area	22.5 mm × 21.8 mm
	Channel width	0.3 mm
	Rib width	0.3 mm
	Channel depth	0.2 mm
Sputtering material	Silver	99.99%
Thin copper plate for current collected	Resistance	1.7×10^{-6} Ω-cm
	Each one cover flow field area	0.5 mm × 21.8 mm
Carbon film resistance		0.1 Ω
	Deviation	0.01 Ω
Anode reactant gas	Hydrogen	99.99%
	Humidity	70%
	Flow rate	10 sccm
Cathode reactant gas	Air	
	Flow rate	60 sccm
Reaction area		22.5 mm × 21.8 mm
Cell operation temperature		25 °C
Cell operation pressure	Anode	97 kPa
	Cathode	97 kPa

2.2. Sample preparation and the test loop

In the present study, four flow channels frequently used in the commercial market: mesh, parallel, serpentine and interdigitated flow type channel with definite rib widths, was micro-fabricated. Fig. 1 also shows the four different flow fields were used in the present experiments with rib width of 150 μm and channel width of 300 μm. Following Hsieh et al. [9], the flow field plates were fabricated with copper metal sheets or silicon wafer depending on which electrode would be measured by using LIGA-like (LIGA; a German acronym for *lithographie galvanoformung abformung*) micro-fabrication process of deep ultraviolet (UV) lithography to obtain SU-8 (2100) resist patterns/and SU-8 mould [9]. A similar micro-fabrication process was used here. The present system uses a segment having an area of 22.5 mm × 4.5 mm each on the cathode or anode side of the cell, with a common collector on the anode or cathode side. The segmented current collector is fabricated using printed circuit board (PCB) technology with 38 mm (l) × 0.5 mm (w) × 0.01 mm (t) copper pin covering on an area of 22.5 mm × 0.5 mm flow channel. Each copper pin is connected to 0.1 Ω carbon film resistor. By Ohm's law, the local current of each segment can be measured within ±0.001 Ω accuracy.

The single PEM fuel cell was built with DuPont Nafion 117 with Pt area density of 0.50 mg cm^{-2} catalyst loading on the anode and cathode electrodes. Two 290 μm carbon papers (ELAT) from E-TEK served as the GDLs and were added to the MEA. A single MEA was used for all five samples, minimizing the discrepancy in activation and ohmic losses between the testing of samples. The surface characteristics of GDLs influence the liquid water distribution, for example, the interfacial liquid water coverage. Prior to each test, the contact angle for the present GDLs was measured and a hydrophobic GDL, proven. One of the measured results (≈127°) is shown in Fig. 2(a).

The computer-controlled single fuel cell system and circulating loop is designed (see Fig. 2(b) for details) for operation with hydrogen and air. The reactant gases are fed in series to the cells. Hydrogen (H_2) and air are conducted parallel flow mode on both the anode and cathode of the single cell. At the anode, the purified hydrogen (99.99%) was supplied at a flow rate of 10 sccm, both in the humidified (RH 70%) and non-humidified cases, while on the cathode code, the air was delivered at a fixed flow rate of 60 sccm. The cell operating pressure on both anode and cathode is 97 kPa and operating temperature is 25 °C.

2.3. Measurements and procedure

The purpose of the measurements is threefold: (1) to demonstrate the ability of the measurement system to map current density distribution from a working micro-PEM fuel cell with four different flow configurations, (2) to examine the effect of water formation on current distribution at both electrodes, especially for the cathode, and (3) to examine the effect of flow field configuration on current distribution. Measurements were performed under constant cell temperature and constant back pressure on both electrodes when ambient conditions were stable. The measurement procedure was the same for all measurements. Since processes on anode and cathode are difficult to distinguish from one another, similar flow fields on both electrodes should be applied for the examination of downstream effects. Therefore, for the measurements reported in this work, an identical flow field design for anode and cathode was used.

Initially, the cell was kept at the designed temperature and pressure (25 °C and 97 kPa) and the humidifier-generated humidity increased to 70% RH with the flow rates of anode at 10 sccm and cathode at 60 sccm, respectively. Then current distributions were measured for each consecutive time interval and after the

Table 2
Measurement uncertainty

Data logger	Agilent 34970A	
	Range	Error
DC volt	100 mV	±6.5 μV
	1 V	±26 μV
	10 V	±190 μV
DC current	10 mA	±1.5 μA
	100 mA	±14 μA
Product water measurement		
Water accumulation percentage	16–48%	±0.85%

cell reached a steady state, a polarization curve was measured. Each measurement was repeated at least four times within the deviation between them being less than ±5%. Finally, average data were then taken and recorded.

2.4. Water accumulation measurement

Water is transported into the cathode by the humidified air, the reaction produced, and the electro-osmotic drag; then it is transported out by the depleted air and back-diffusion. Water is transported into the anode by humidified hydrogen and the back-diffusion through the membrane; then it is transported out by depleted hydrogen and electro-osmotic drag. Generally, water formation can occur at the electrode, GDL, and the flow channel. Here, we focus on water accumulating in both electrodes, especially in the cathode that primarily determines cell performance.

An operational micro-PEM fuel cell with flow fields of mesh, parallel, serpentine, and interdigitated configuration was used to fulfill the present water accumulation measurements. Photo images show the area of 22.5 mm × 22.5 mm and were taken at different times upon dissembling the fuel cell. Both counter flow and concurrent flow to the anode and cathode were applied in all cell tests. A digital camera (Fuji film, FinePix F40fd) was used for imaging (10 frame min^{-1}). Both the anode and cathode side were observed and the data were examined and analyzed because liquid water buildup on the anode side may still occur as previously stated due to the unused hydrogen reaching saturation before leaving the cell and back-diffusion through the membranes from the cathode side. Table 2 lists the degrees of uncertainty regarding the relevant parameters and variables measured in this study.

3. Results and discussion

3.1. Local current density distribution

3.1.1. Short transient ($t \leq 5$ s)

The local current density distribution measurements on the cathode provide a map of those locations that are starved of air (oxygen). Fig. 3 shows the current distribution on the cathode for the initial 5 s after the cell starts up for the four different flow configurations studied herein. The airflow direction, which is from bottom to top, is marked in the figures with an arrow. The most original current density evolution/history on the entire channel can be clearly seen with different color transitions. Some common features are observed. Generally, the local current density is higher at the inlet region and decreases along the downstream flow channel towards the outlet due to the consumption of the reactant gas. Higher current density near the inlet causes a higher air (oxygen) consumption rate and a lower air (oxygen) concentration downstream. Among the four flow fields, the serpentine flow channel shows the most uniform local current distribution over the entire flow channel followed consecutively by interdigitated, mesh and parallel flow channel. However, for cell performance, a limiting current density of 300 mA cm^{-2} can be completely attained for interdigitated flow channel at about the initial 2 s, with an average limiting current density of 277 mA cm^{-2} throughout the entire flow field. On the other hand, serpentine would give an average (based on the active area) limiting current density of 247 mA cm^{-2}, while mesh flow field presents the worst, of about 215 mA cm^{-2}. The reasons may be due to the water formation, accumulation, and flooding, which will be further explained and in greater detail, later.

Furthermore, reactant depletion can occur through one of the following means, which include: upstream utilization of air leaving the downstream channel without sufficient reactant feed, blockage of a flow field channel due to liquid water formation, and different flow field design to prevent the reactant from access to the cathode as well as to hinder the removal of liquid water. Generally speaking, the present four flow fields seem to provide a relatively smooth local current density distribution, which means that the airflow is strong enough to form fairly homogenous oxygen concentration along the flow channel in the short transient ($t \leq 5$ s).

3.1.2. Long time period ($1 \leq t \leq 180$ min)

For time period greater than 1 min, Fig. 4 shows the time evolution of the local current distribution on the cathode for four different flow field configurations. As one can see, the current density distribution remains relatively stable for four different flow fields to the maximum operating time of 180 min.

To elucidate the local current distribution of the fuel cell and the comparison between the cathode and anode side, the local current distribution on the anode is shown in Fig. 5. This can be seen according to the length of time, and it would take to attain the corresponding limiting current density. Basically, the local current density on the cathode and anode should be identical with some experiment error found as expected.

Among four different flow fields, both serpentine and interdigitated flow channel provide a fast response for a smooth and uniform current density distribution within 1 s. In spite of the lower response of the mesh and parallel flow channel, all flow fields (including mesh/parallel), would reach a stable and uniform current density distribution over the entire flow channels as time goes on and surpasses 5 s.

In fact, based on the design of the channel flow passage, the reactant gas in PEM fuel cell with interdigitated flow channels is driven by forced convection with a higher pressure drop between the inlet and outlet of the channel. By switching from a diffusion driven to a convection-driven mass transport process, the cathode reaction rates can be significantly enhanced. Such behavior would be obviously dominatant with a better mixing/reaction effect of catalyst and reactant gas in the interdigitated flow fields in the present study. The superior performance can also be attributed to the combined effects of a convective transport mechanism for the reactant gas together with a better distribution with respect to these of other flow fields over the entire flow area. With these reasons above, the interdigitated flow channel showed the highest current density and the most uniform distribution among the four flow fields under study. Meanwhile, the pressure drop through the inlet to the outlet for these four flow fields was measured (not shown). The highest pressure drop across the cathode flow channel for interdigitated flow field was found. Furthermore, such high pressure at the upper half channel seems of insignificance on the current density. Further study may include this aspect.

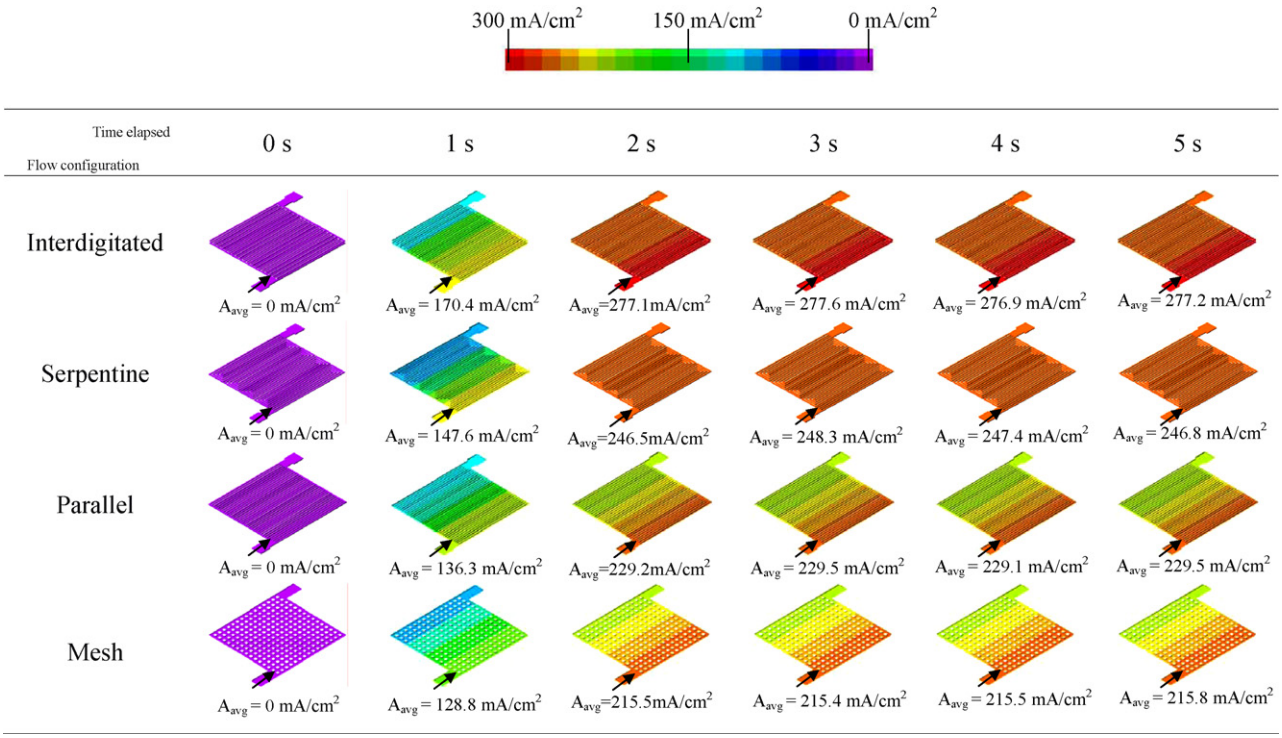

Fig. 3. Current density distribution measurement on cathode side for four different configuration at initial 5 s.

3.2. *Current density/water distribution upon VI/PI curves recording*

Fig. 6 shows the cathode flow field current density distribution compared at similar voltage while recording the VI/PI curves. Initially, the current density is zero/or near zero for all four flow fields at the same cell voltage (V = 0.87 V). When switching cell voltage from 0.87 to 0.41 V, the average current density of the interdigitated flow field becomes 173.5 mA cm^{-2}, which is the biggest, followed by 156, 140, and 122.6 mA cm^{-2} for serpentine, parallel, and mesh flow field, respectively. This situation prevails even at 0.17 V, in which the average current density reaches 277.1 mA cm^{-2} for the inter-

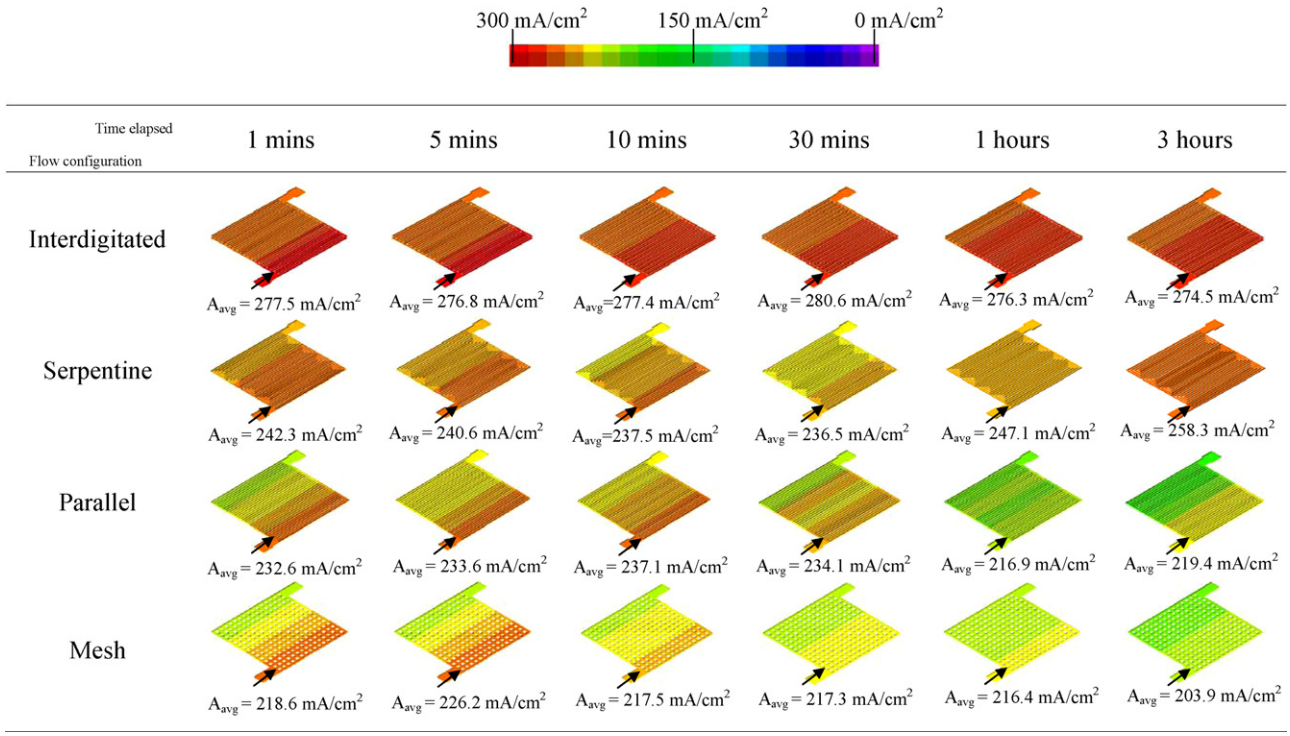

Fig. 4. Current density distribution evolution on cathode side for four different configuration.

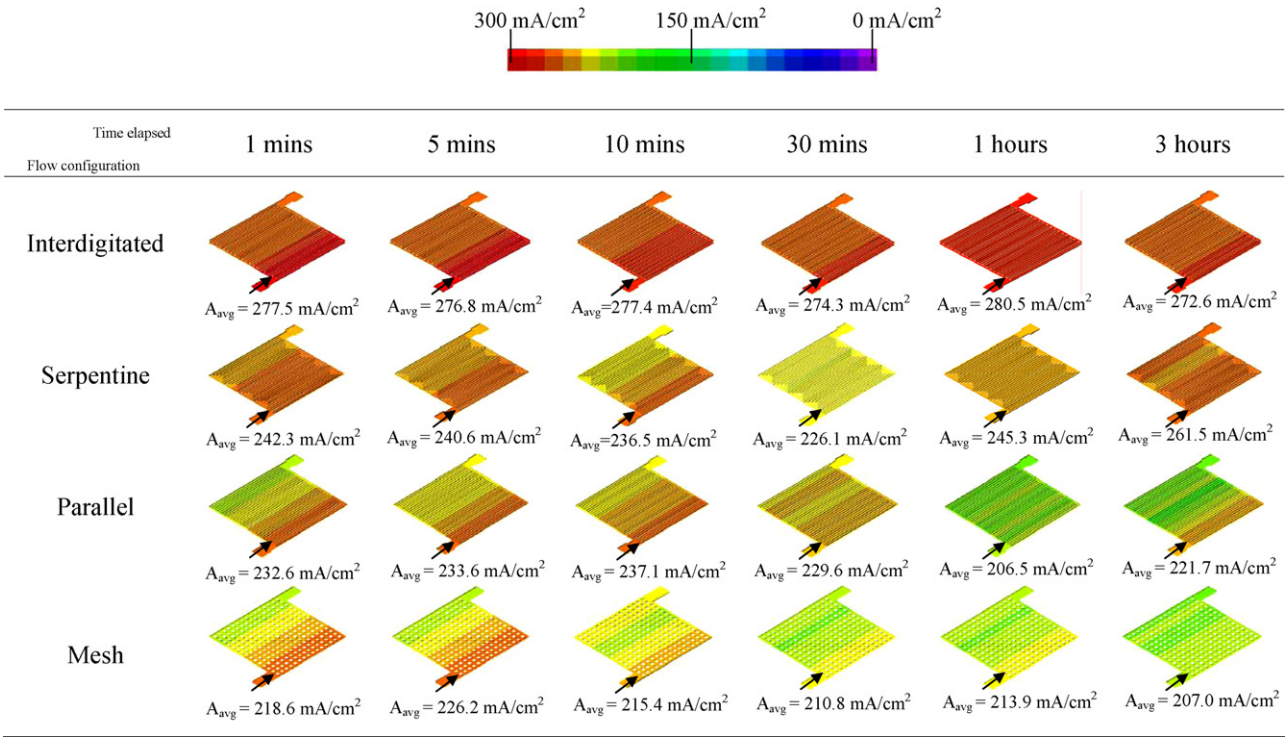

Fig. 5. Current density distribution evolution on anode side for four different configuration.

digitated flow channel. Again, the smallest valu is 207.4 mA cm^{-2} for the mesh flow channel. All of these can be evidenced from the corresponding VI/PI curves, as also shown in Fig. 6.

Similarly, cathode flow field water distribution compared at similar current density while recording the VI/PI curves, is shown in Figs. 7 and 8 at t = 30 and 180 min, respectively. At the cell voltage (V) = 0.11 V, liquid water formed and accumulated from left to right of the flow channel as shown in Fig. 7(a)–(d). During the evolution of liquid water in the flow channels, condensation plays an important role in the emergence of water formation. Fog was initially observed on the floor of the flow channels consisting of myriad tiny water droplets which grow and finally accumulate in the flow channels. Some small water droplets coalesce to become large droplets. However, water columns do not appear to occur. The water production from the oxygen reduction reaction is based on the cell operating current density, following Faraday's law. At a higher current density, the water formation in the flow channel is more serious than that at a lower current density.

The water flooding problems for the interdigitated flow channel are more severe than the case is for the other three channels. The volume of water in the flow channels is about 27%, which is much higher than those (≈17%) of serpentine, parallel and mesh flow channels. However, when operating average current density switches from I_{avg} = 275–210 mA cm^{-2} (at V = 0.12 V), the water formation seems to stop and water content reaches a nearly constant value (≈45 vol.% on average for the four channels) as shown in Fig. 8(a)–(d). From Figs. 7 and 8, the local water distribution in the entire flow field was non-uniform and almost all the liquid water appeared at the downstream end of the flow field as the liquid water does not appear until the water vapor reaches saturation. Since water distribution and current density distribution are coupled, non-uniform water distribution would result in a corresponding non-uniform current density distribution, as evidenced by Figs. 7 and 8. Moreover, Figs. 7(a), (c), and (d) and 8(c), clearly indicate that when quite a bit of liquid water appears, the upstream flow channel produces higher current densities.

It is known that the role of the flow field is to distribute the reactants to the catalyst-coated membrane as uniformly as possible and with minimum mass transport limitations. The superiority of a certain flow field upon others is therefore detected at higher current density, especially in the transport polarization regime. It appears from Figs. 6–8 that, in the present experiments, current densities around 200 mA cm^{-2} correspond to the mass transport limitation regime. Although the interdigitated flow field has been proven to be better than the others, its performance was still low as compared to those of previous studies of conventional large PEM fuel cells. This is perhaps because the present study of the micro-PEM fuel cell is operated at a low temperature of 25 °C for cell phone applications.

3.3. Cathode/anode water distributions

Generally, once the electrochemical reaction takes place, the water production would occur in the flow channel. It initially looks foggy. Over time, these fog would accumulate and coalesce to become some small droplets with an initial size of about 100 μm on the channel floor. They were pushed by airflow in the cathode flow channel, and moved toward the outlet of the channel. Consequently, most of these was collected in the corner of the channel and would become bigger, and finally fulfill the flow channel. Soon thereafter, the flooding emerges and locates at the bottom left corner of the channel. The flooding area would become larger as time goes by. The water production from the oxygen reduction reaction is based on the cell current density, following Faraday's law. At a higher current density, the water formation in the flow channel is more serious than that at a low current density. Detailed evolution of the water formation, flooding, and liquid volume fraction are described below.

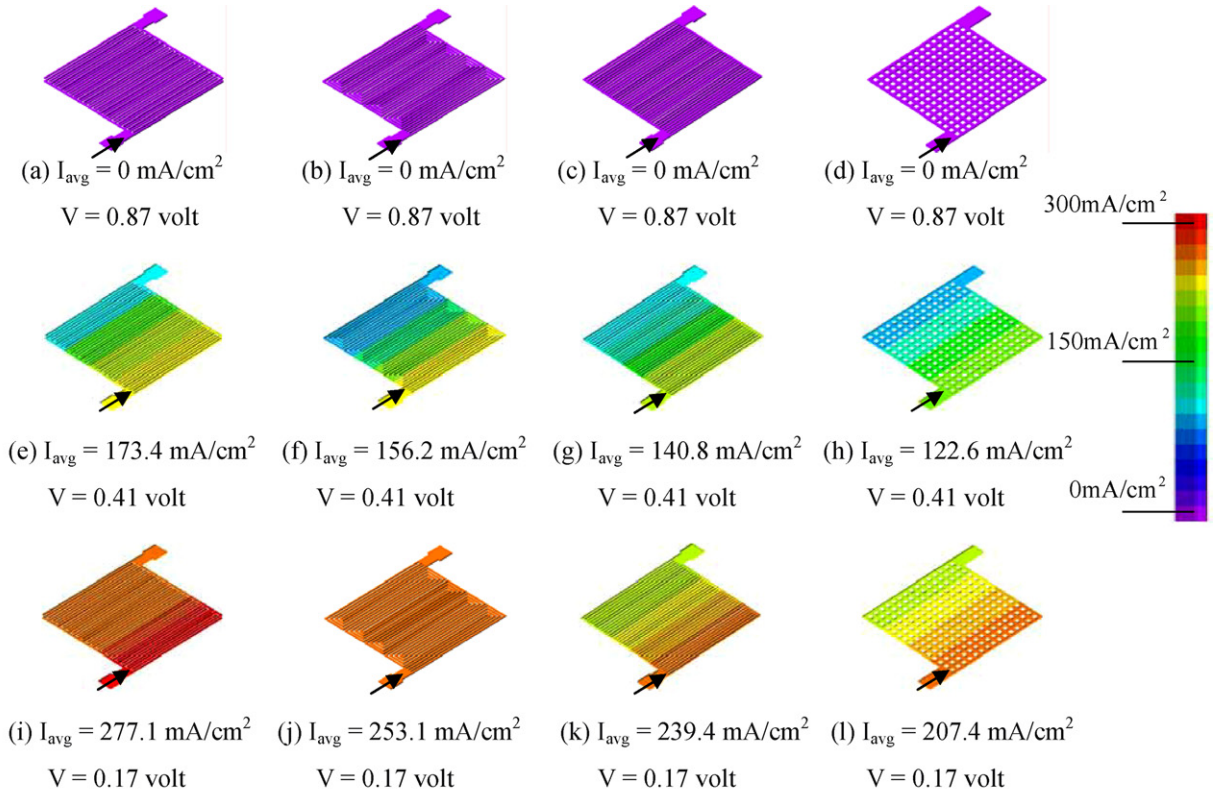

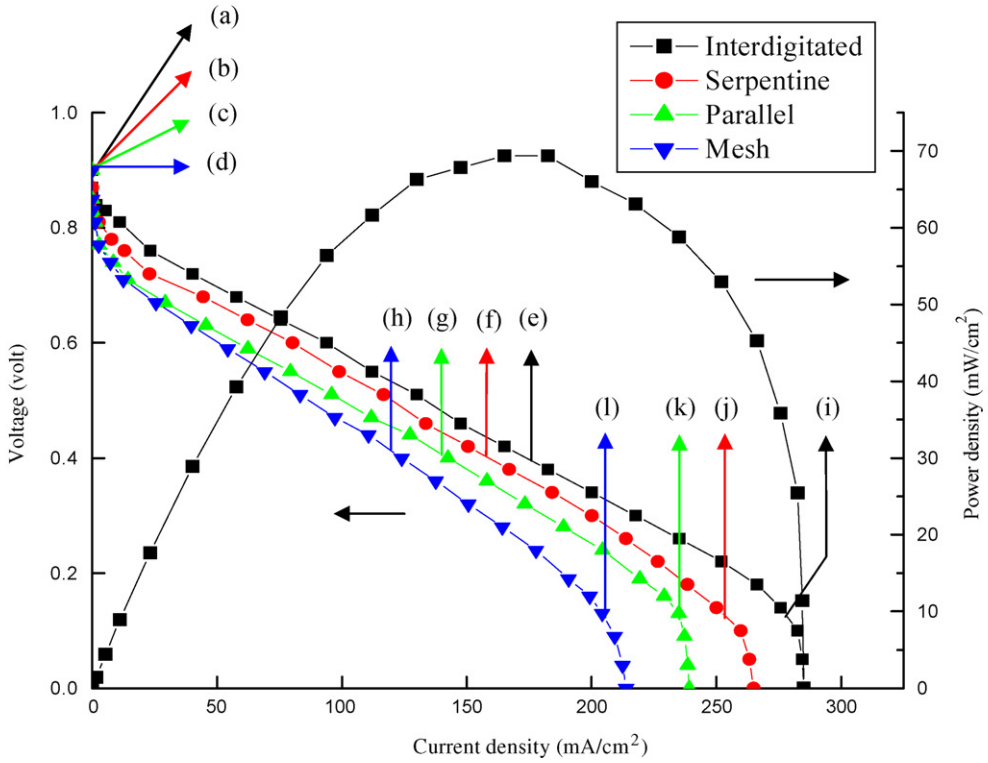

Fig. 6. Comparison of flow fields at same operating conditions. (a)–(d); (e)–(h); and (i)–(l) cathode current density distribution compared at a similar voltage.

In Fig. 9, at t = 5, 10, 15, 20, and 25 min, the liquid water formation, accumulation, and flooding can be clearly seen and identified for the four flow fields at the cathode side. Fig. 9(a) shows the image of local liquid water distribution over the entire active area with the product water volume fraction at different times. Droplet formation was clearly noted and identified with a size of about 100 μm in diameter. As time progresses, the liquid water volume fraction increases. The water flooding front moves from the bottom left cor-

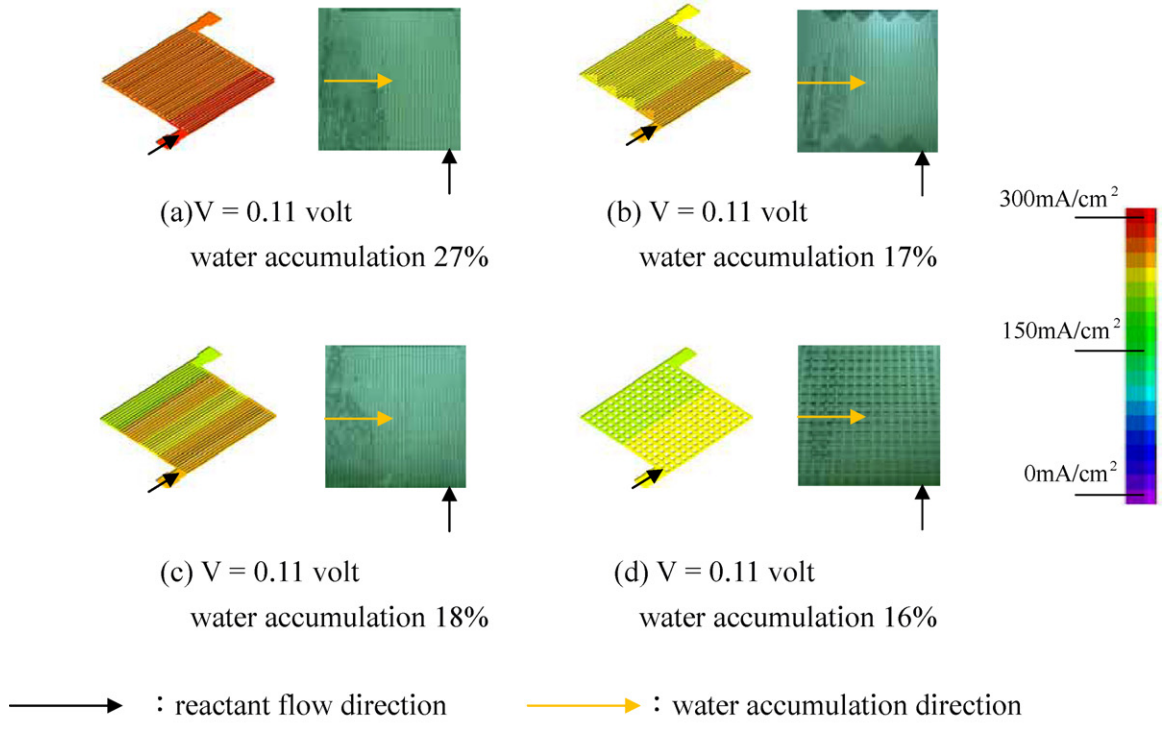

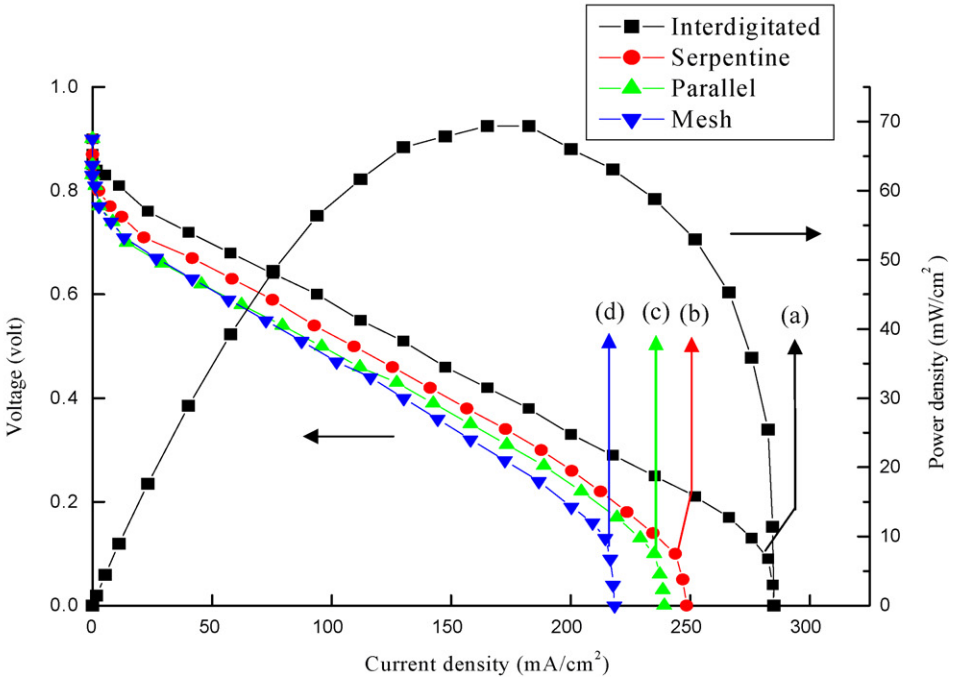

Fig. 7. Four cathode flow fields flooding compared at similar current density while recording the polarization curves after operating 30 min.

ner to the upper right corner, with water bubble evolution sequence of the water droplet, condensation, and, finally fogging. Fig. 9(b)–(d) follows the same trend for serpentine, parallel, and mesh type flow fields. The nearly similar product water evolution behavior occurs with a slightly higher product water volume fraction about 20% at $t = 25$ min for the interdigitated flow channel. To avoid the difficulty of measurements and calculations for the liquid volume fraction via the photo image technique, extreme care and caution were taken to keep the associated uncertainty to minimum.

Water content at both the cathode and anode sides at $t = 30$ and 180 min, are shown in Fig. 10, respectively, for the four different flow fields. Again, the water formed consistently from left to right all over the entire flow channel as stated before. Several origins of liquid water within both the cathode and anode channels were observed. Liquid water is expelled through GDL pores into the channels. The occurrence of condensation or fogging on the channel was observed. Note that no water was observed at the open circuit. Furthermore, no water could be

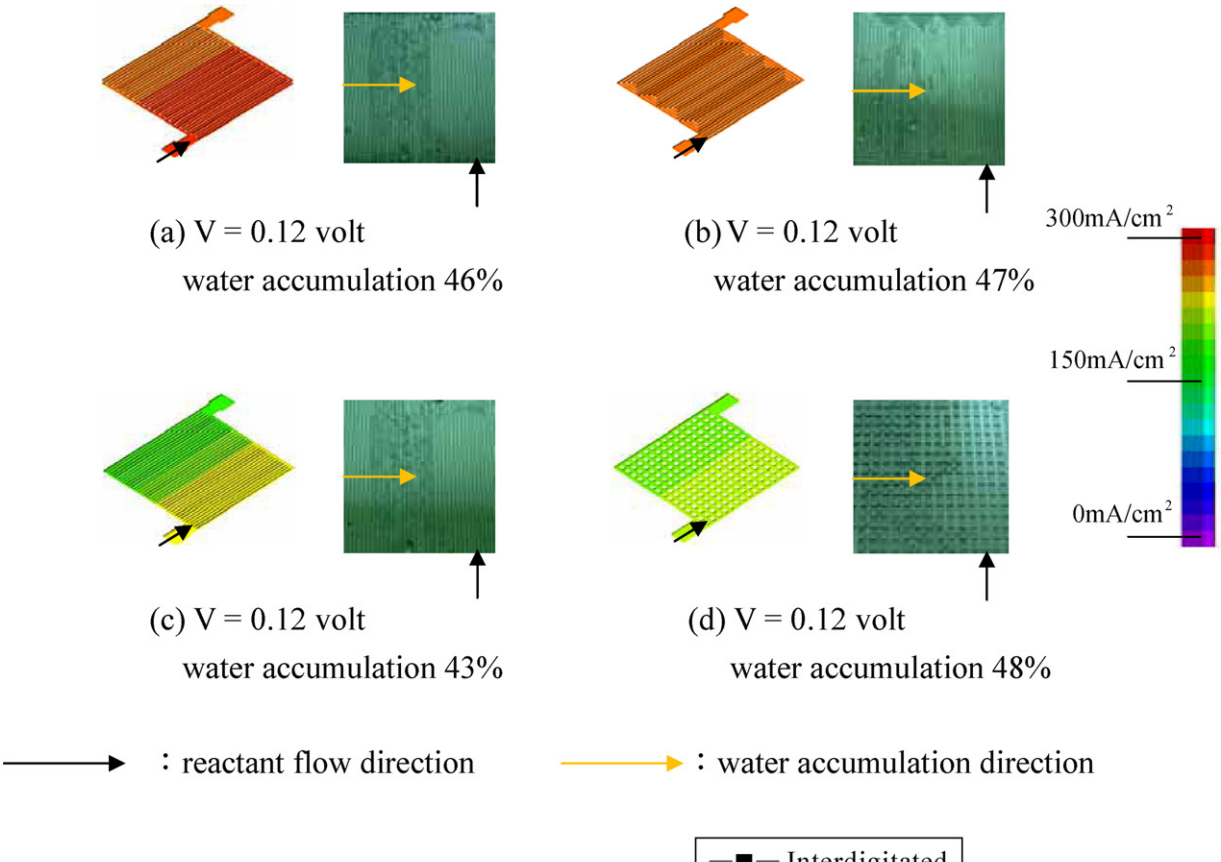

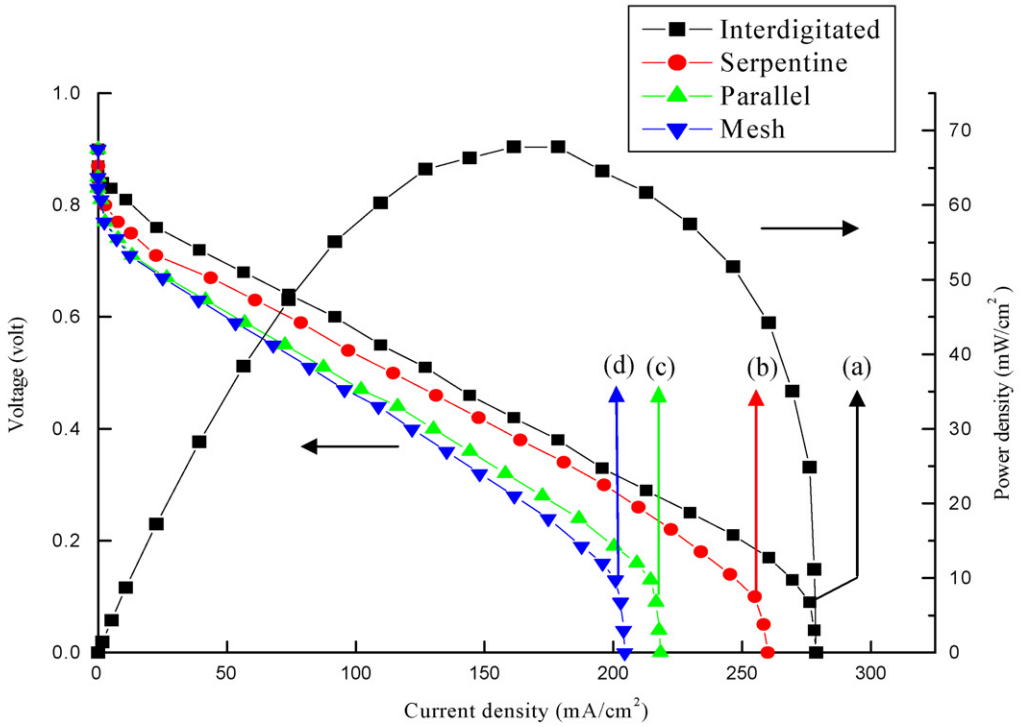

Fig. 8. Four cathode flow fields flooding compared at similar current density while recording the polarization curves after operating 180 min.

seen unless an onset current density was reached, which was found to be 100 mA cm^{-2} in the present case. Occasional bursts of liquid water, accompanied by instantaneous fogging from the test channels, were also noted. Water transport occurs due to the high inlet air velocity and droplets growing from the GDL pores being removed by the air stream. In addition, the droplets are often swept away by other droplets, slugs and film that originated from the upstream water accumulation. Not much area coverage was observed, which might be due to the present hydrophobic GDLs, indicating that the discrete water droplet formation occurs periodically at preferential locations, rather than liquid water spread out on the GDL surface. Generally, anode water flooding is clearly less serious than that of on cathode.

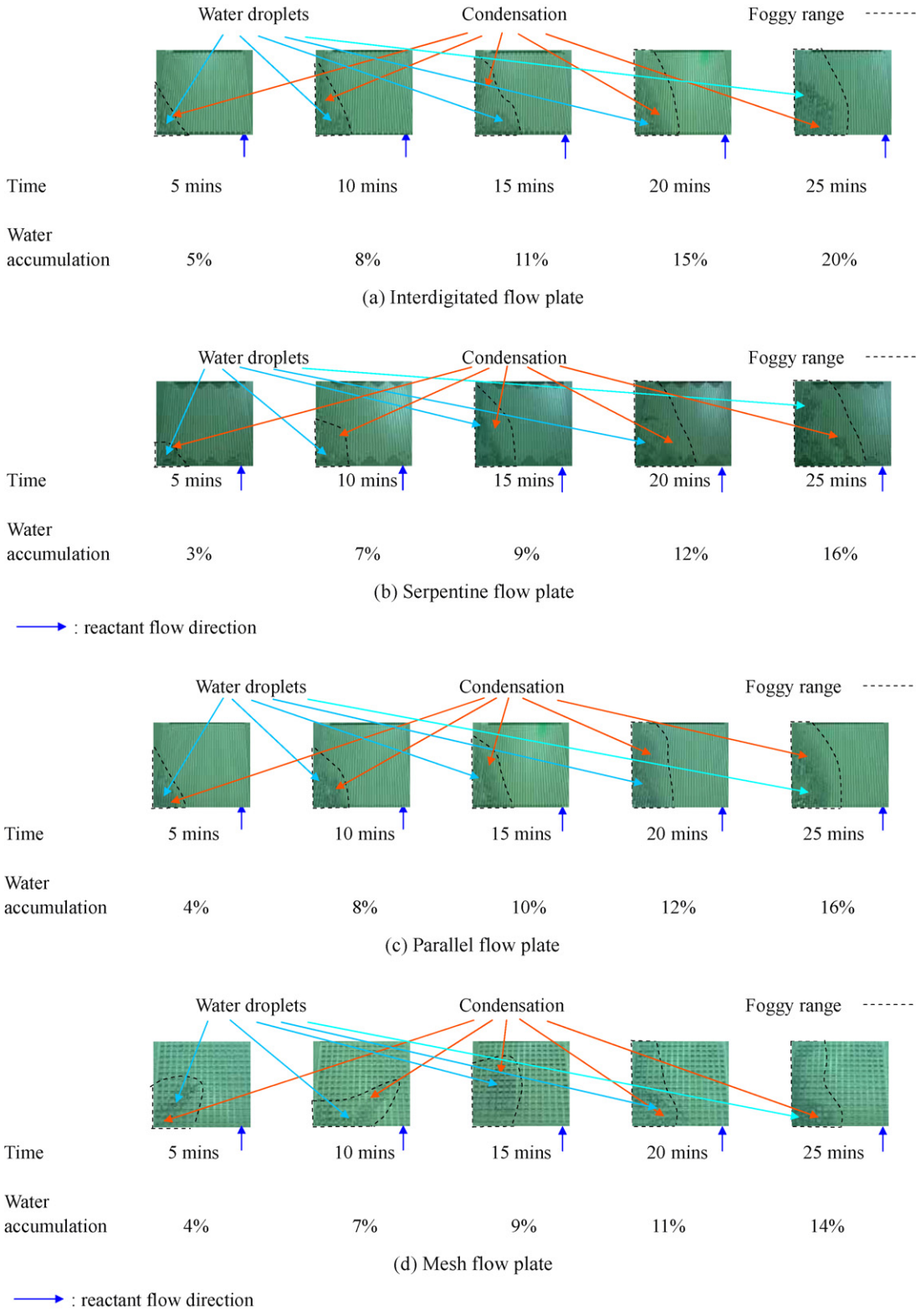

Fig. 9. Water formation images ($5 \le t \le 25$ min) on cathode for different flow channels.

3.4. Correlation of liquid volume vs. time (t)

As stated previously, liquid water first accumulates in the GDL and at an initial dry state. Once the GDL reaches a critical saturation fraction, the bulk of liquid water is ejected into the channels in the form of droplets. This behavior is characterized by the time rate change in measured liquid water volume as depicted in Fig. 11. Results shown in the inset are the water content measurement after dissembling the fuel cell with the corrections made for water evaporation of the airflow while the experiments progress. Fig. 11 illustrates a nearly linear relationship between liquid water volume and the progressive time (t). Since the airflow is very sensitive to

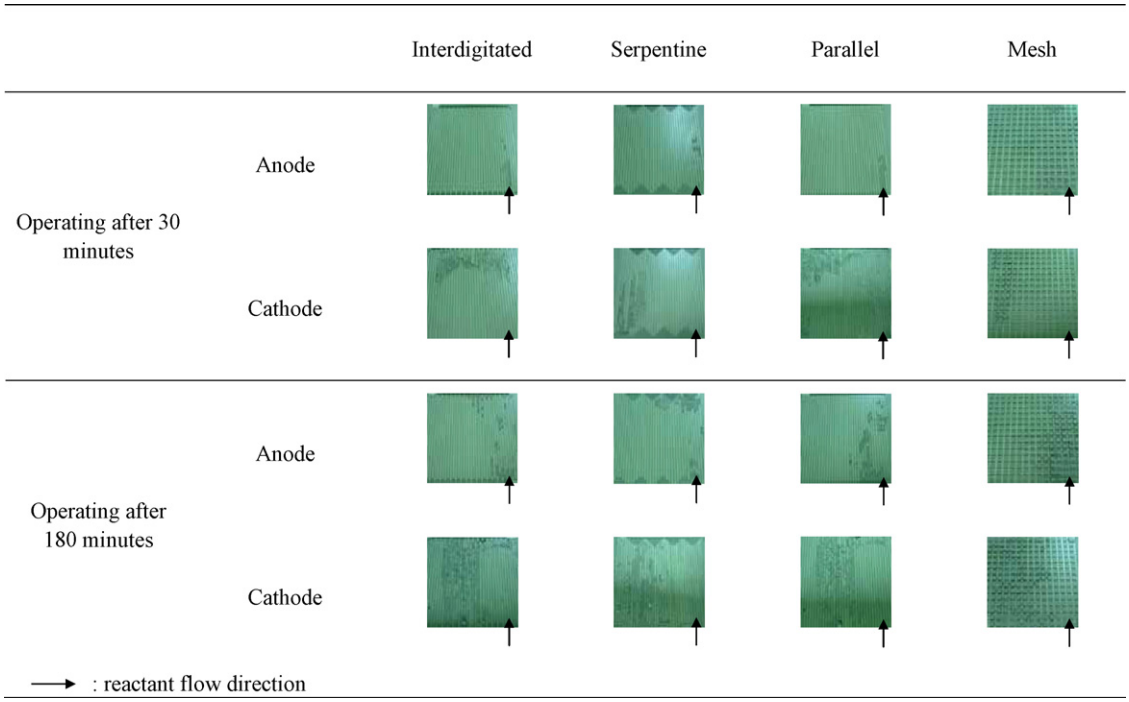

Fig. 10. Water accumulation images for anode and cathode for four different flow fields after the fuel cell operating at 30 and 180 min, respectively.

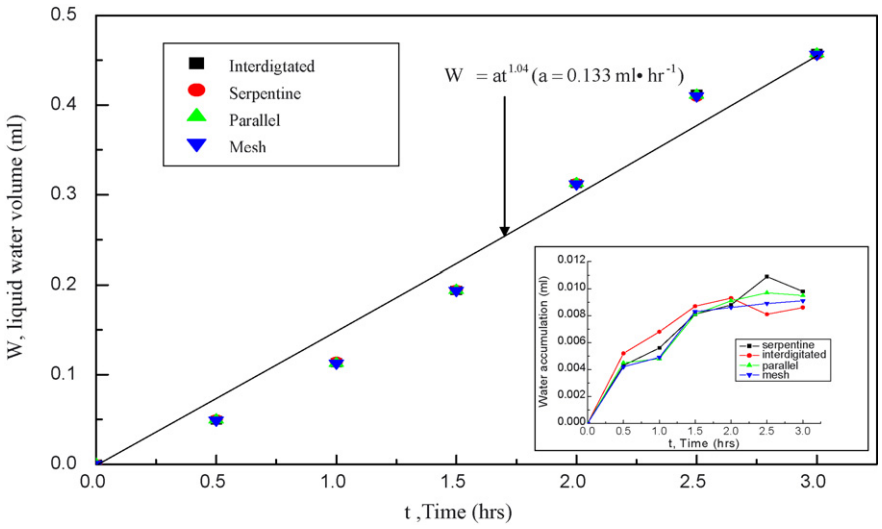

Fig. 11. Cathode water accumulation (after correction) for four different flow fields (inset indicating the water accumulation measured).

small blockage due to the water formation, this is thought to initiate an inadequate oxygen concentration on the cathode for mesh and parallel flow fields as discussed earlier.

4. Conclusions

Direct in situ measurement of transient local current density distribution and estimation of liquid water accumulation on both anode and cathode from an H_2/air micro-PEM fuel cell with mesh, parallel, serpentine, and interdigitated flow fields, are achieved and presented.

(1) An interdigatated flow filed would give the most uniform and the highest local current density compared to those of mesh, parallel, and serpentine flow fields during the entire time period (i.e. $0 \le t \le 3$ h) under study.
(2) As time approaches 30 min, all four flow fields would obtain a nearly steady-state local current density distribution. As time goes on ($\le$3 h), local current density decreases due to liquid water formation and flooding.
(3) The product water formation at the cathode side cannot be seen until $t \ge 5$ min for all the four flow fields under study. The water bubble formation follows the sequence of: water droplet, condensation, and finally fogging with the maximum droplet size of 100 μm in diameter.
(4) The product water is proportional to the local current density, which indicates that the interdigitated flow field would have the largest amount of liquid water in channels (≈27%)

at $t = 30$ min. However, it would nearly reach a constant volume fraction of 45% of the product water for four flow fields at $t = 180$ min.

(5) A simple correlation with a linear relationship of the amount of water accumulation in the flow channels with time is developed.

References

[1] M. Noponen, T. Mennolc, M. Mikkola, T. Hottinen, P. Curnd, J. Power Sources 106 (2002) 304–312.
[2] S.J.C. Cleghorn, C.R. Derouin, M.S. Wilson, S. Gottesfeld, J. Appl. Electrochem. 28 (1988) 663–672.
[3] J. Stumper, S.A. Campbell, D.P. Wilkinson, M.C. Johnson, M. Davis, Electrochim. Acta 43 (1998) 3773–3783.
[4] Ch. Wieser, A. Helmbold, E. Gtilzow, J. Appl. Electrochem. 30 (2000) 803–807.
[5] G. Bender, M.S. Wilson, T.A. Zawodzinski, J. Power Sources 123 (2003) 163–171.
[6] J. Larminie, A. Dicks, Fuel Cell Systems Explained, 2nd ed., John Wiley, England, 2003, pp. 94–96.
[7] S.-S. Hsieh, S.-H. Yang, J.-K. Kuo, C.-F. Huang, H.-H. Tsai, Energy Convers. Manage. 47 (2006) 1868–1878.
[8] H. Nakajima, T. Konomi, T. Kitahara, J. Power Sources 171 (2007) 457–463.
[9] S.-S. Hsieh, C.-L. Feng, C.-F. Huang, J. Power Sources 163 (2006) 440–449.